Decreased Lamina Cribrosa Beam Thickness and Pore Diameter Relative to Distance From the Central Retinal Vessel Trunk

Bo Wang,[1,2] Katie A. Lucy,[1] Joel S. Schuman,[1,2,3] Ian A. Sigal,[1,2] Richard A. Bilonick,[1,4] Larry Kagemann,[1,2] Tigran Kostanyan,[1] Chen Lu,[5] Jonathan Liu,[5] Ireneusz Grulkowski,[5] James G. Fujimoto,[5] Hiroshi Ishikawa,[1,2] and Gadi Wollstein[1,2]

[1]Department of Ophthalmology, University of Pittsburgh School of Medicine, UPMC Eye Center, Eye and Ear Institute, Ophthalmology and Visual Science Research Center, Pittsburgh, Pennsylvania, United States
[2]Department of Bioengineering, Swanson School of Engineering, University of Pittsburgh, Pittsburgh, Pennsylvania, United States
[3]Department of Ophthalmology, New York University School of Medicine, New York, New York, United States
[4]Department of Biostatistics, University of Pittsburgh School of Public Health, Pittsburgh, Pennsylvania, United States
[5]Department of Electrical Engineering and Computer Science, Massachusetts Institute of Technology, Cambridge, Massachusetts, United States

Correspondence: Joel S. Schuman, NYU Langone Medical Center, 462 First Avenue, NBV 5N3, New York, NY 10016, USA; joel.schuman@nyumc.org.

Submitted: December 23, 2015
Accepted: April 27, 2016

Citation: Wang B, Lucy KA, Schuman JS, et al. Decreased lamina cribrosa beam thickness and pore diameter relative to distance from the central retinal vessel trunk. *Invest Ophthalmol Vis Sci*. 2016;57:3088–3092. DOI:10.1167/iovs.15-19010

Purpose. To investigate how the lamina cribrosa (LC) microstructure changes with distance from the central retinal vessel trunk (CRVT), and to determine how this change differs in glaucoma.

Methods. One hundred nineteen eyes (40 healthy, 29 glaucoma suspect, and 50 glaucoma) of 105 subjects were imaged using swept-source optical coherence tomography (OCT). The CRVT was manually delineated at the level of the anterior LC surface. A line was fit to the distribution of LC microstructural parameters and distance from CRVT to measure the gradient (change in LC microstructure per distance from the CRVT) and intercept (LC microstructure near the CRVT). A linear mixed-effects model was used to determine the effect of diagnosis on the gradient and intercept of the LC microstructure with distance from the CRVT. A Kolmogorov-Smirnov test was applied to determine the difference in distribution between the diagnostic categories.

Results. The percent of visible LC in all scans was 26 ± 7%. Beam thickness and pore diameter decreased with distance from the CRVT. Glaucoma eyes had a larger decrease in beam thickness (−1.132 ± 0.503 μm, $P = 0.028$) and pore diameter (−0.913 ± 0.259 μm, $P = 0.001$) compared with healthy controls per 100 μm from the CRVT. Glaucoma eyes showed increased variability in both beam thickness and pore diameter relative to the distance from the CRVT compared with healthy eyes ($P < 0.05$).

Conclusions. These findings results demonstrate the importance of considering the anatomical location of CRVT in the assessment of the LC, as there is a relationship between the distance from the CRVT and the LC microstructure, which differs between healthy and glaucoma eyes.

Keywords: optical coherence tomography, blood vessel, glaucoma

The lamina cribrosa (LC) is considered to have an important role in the pathogenesis of glaucoma,[1,2] the second leading cause of blindness worldwide.[3] Mechanical deformation of the LC, a connective tissue meshwork, is thought to result in a biological cascade that leads to the death of the retinal ganglion cell axons that pass through the meshwork.[1] Therefore, the LC has been a subject of active investigation and a number of studies have identified ex vivo and in vivo differences between the healthy and glaucomatous LC.[2,4–6]

Several structural components of the LC have been studied for their role in glaucoma pathogenesis.[4,5,7,8] However, the central retinal vessel trunk (CRVT) that pierces the LC has been relatively ignored in both modeling and human studies, despite indications that it may be important in glaucoma. The CRVT can potentially contribute to its biomechanical properties. Funduscopic studies by Jonas et al.[9] have demonstrated that neuroretinal rim loss and peripapillary atrophy[10] occurred in the disc periphery farthest away from the CRVT.

Building on previous findings, we hypothesize that the distance from the CRVT within the LC affects the LC microstructure—specifically the pores through which retinal ganglion cell axons pass on their path from the eye to the brain and the beams that provide structural support and nutrition for those axons. Specifically, we investigated the in vivo relationship between LC microstructure and the CRVT location using optical coherence tomography (OCT), which offers a unique opportunity for quantifying LC microstructure in three dimensions (3D) due to its high axial and lateral resolution.

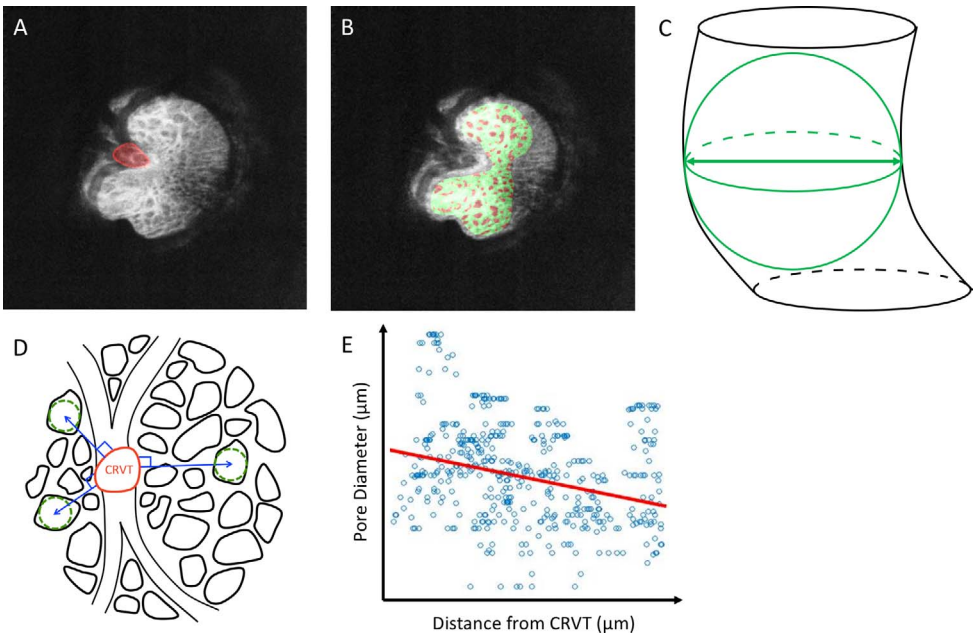

Figure 1. (**A**) En-face slice of the LC with the CRVT manually delineated (*red*). (**B**) Automated segmentation showing the beams (*green*) as well as the pores (*red*) on a single C-mode slice from the 3D stack. (**C**) Schematic diagram demonstrating the quantification of pore (*black*) by local thickness defined in 3D (*green*). (**D**) Schematic diagram demonstrating the method of determining how LC pore diameter (*green dashed lines*) varied with distance from the CRVT (*blue lines*). (**E**) A linear fit (*red line*) of the association between pore diameter and distance from CRVT for a single eye.

Methods

The study was conducted in accordance with the tenets of the Declaration of Helsinki and the Health Insurance Portability and Accountability Act. The institutional review board of the University of Pittsburgh (Pittsburgh, PA, USA) approved the study. All subjects gave written informed consent prior to participation in the study.

Subjects were consecutively recruited from the Pittsburgh Imaging Technology Trial carried out at the University of Pittsburgh Medical Center Eye Center. One hundred nineteen eyes (40 healthy, 29 glaucoma suspect, and 50 glaucoma) from 105 subjects were enrolled to the study. All participants underwent a comprehensive ophthalmic examination, including slit-lamp biomicroscopy, IOP measurement and funduscopy, visual field testing (Swedish interactive threshold algorithm standard 24-2 protocol; Humphrey visual field analyzer, Zeiss, Dublin, CA, USA), and imaging with swept-source (SS-) OCT. Healthy eyes were defined as those having a normal optic nerve head (ONH), retinal nerve fiber layer, and full visual fields without any previous history of retinal pathology or glaucoma. Glaucoma suspects were defined as those having suspicious optic nerve or retinal nerve fiber layer appearance, or IOP greater than 21 mm Hg, but without corresponding visual field abnormalities. The contralateral eye of subjects with glaucoma was classified as glaucoma suspect, if it appeared to be normal. Glaucomatous eyes were classified by characteristic glaucoma damage to the optic nerve and retinal nerve fiber layer with corresponding visual field loss. If both eyes were eligible, both were included in the appropriate category.

All eyes were scanned using a $3.5 \times 3.5 \times 3.64$–mm volume centered on the ONH using a previously described custom-built swept SS-OCT device.[11] The SS-OCT featured a 1050-nm central wavelength with a 100-kHz scan rate. The device has an axial resolution of 5 μm and lateral resolution of 20 μm in the eye. Two orthogonally oriented scan volumes were obtained sequentially for each eye and registered to reduce motion artifacts.[12] The LC microstructure of each eye was automatically segmented using a previously described method with high reproducibility.[13,14] The diameter of LC pores and the thickness of LC beams were defined by the 3D local thickness (Fig. 1)[4,14,15] using the BoneJ[16] plugin of ImageJ software (http://imagej.nih.gov/ij/; provided in the public domain by the National Institutes of Health, Bethesda, MD, USA).[17]

The CRVT was manually delineated at the level of the center of the visible LC depth (Fig. 1A). Using MATLAB (Mathworks, Natick, MA, USA), an euclidian distance map was generated from the margin of the CRVT to each individual pore and beam. A linear fit was applied to the distribution of LC microstructure (pore diameter or beam thickness) with distance from the CRVT (Fig. 1C). Both the gradient (how LC microstructure changes with distance) and the intercept (LC microstructure at the CRVT margin) of the distribution were computed. It is important to note that because the gradient represents the micron change in LC microstructure per micron distance from the CRVT, gradient is a unitless term.

A linear mixed-effects model was used to determine the effect of diagnosis on the gradient and intercept of the distribution of LC microstructure with distance from CRVT, with the percent of visible LC and age serving as a covariate and representing the random effect based on the subject's eye. The linear mixed-effects model accounted for the expected autocorrelation from the use of both eyes in some subjects. The visible LC was defined as the percentage of LC visible compared with the Bruch membrane opening (BMO). The BMO was identified in the cross sections and drawn on a maximum intensity projection image of the ONH. Nonsignificant covariates were removed from the analysis if removing them improved the Akaike information criterion (AIC), a measure of model fit while accounting for model complexity.[18] A Kolmogorov-Smirnov test was applied to determine the difference in distribution between the diagnostic categories. All statistical analysis was performed using R Language

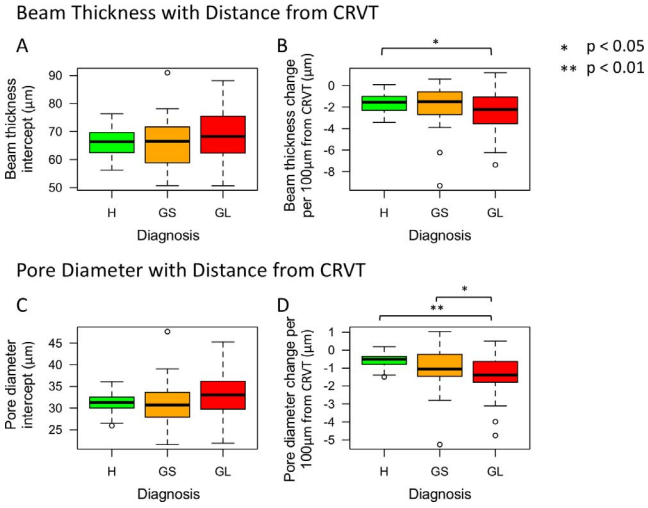

FIGURE 2. Boxplot of (**A**, **C**) intercept and (**B**, **D**) gradient for beam thickness and pore diameter versus distance from the CRVT, respectively, among the clinical diagnostic groups (H, healthy; GS, glaucoma suspect; GL, glaucomatous eyes). Gradient denotes the micron change in lamina cribrosa microstructure (beam thickness or pore diameter) per 100-µm distance from the CRVT.

and Environment for Statistical Computing (version 3.2.0; in the public domain, http://www.R-project.org).[19] Finally, the relationship between the intercept and gradient for both beam thickness and pore diameter, as well as how pore diameter gradient versus CRVT was related to beam thickness gradient versus CRVT, were assessed using a linear mixed-effect model with age and percent of visible LC serving as covariates.

RESULTS

Study Characteristics

The average age of healthy, glaucoma suspect, and glaucoma subjects was 40.2 ± 12.9, 60.7 ± 8.0, and 68.1 ± 14.0 years (mean ± SD), respectively. Age was not a statistically significant parameter in the linear mixed-effect models, did not improve (decrease) the AIC, and was subsequently excluded from the analysis. Average visual field mean deviation for healthy, glaucoma suspect, and glaucomatous eyes was –0.90 ± 1.21, –0.09 ± 0.85, and –7.70 ± 6.92 dB, respectively. Average 3D beam thickness was 58.8 ± 3.6, 59.8 ± 4.2, and 59.3 ± 3.9 µm for healthy, glaucoma suspect, and glaucoma subjects, respectively. Average 3D pore diameter was 28.3 ± 1.6, 27.9 ± 2.2, and 27.6 ± 2.0 µm for healthy, glaucoma suspect, and glaucoma subjects, respectively.

Relationship Between LC Microstructure and Distance From CRVT

The percent of visible LC in all scans was 26 ± 7%. After accounting for the percent of visible LC, both beam thickness and pore diameter decreased with distance from the CRVT, regardless of diagnostic category (Figs. 2, 3). Glaucomatous eyes had a greater decrease in beam thickness (–1.132 ± 0.503 µm, [mean ± standard error] $P = 0.028$) and pore diameter (–0.913 ± 0.259 µm, $P = 0.001$) per 100-µm distance from the CRVT compared with healthy eyes (Table). Glaucomatous eyes also had a greater decrease in pore diameter relative to the distance from the CRVT compared with glaucoma suspects ($P = 0.043$, Table). There was no statistically significant difference in the intercepts between healthy, glaucoma suspect, and glaucomatous eyes.

Glaucomatous eyes had a higher variability in beam thickness gradient versus CRVT ($P = 0.029$) and pore diameter gradient versus CRVT ($P = 0.002$) compared with healthy eyes (Figs. 2B, 2D, and 3). Otherwise, there was no difference in the variability in the gradients or intercepts between the other diagnostic groups.

Lamina cribrosa with thick beam and large pore diameter at the CRVT margin (reflected by high intercepts) were associated with more negative LC beam thickness gradient (Fig. 4A, $P < 0.001$) and pore diameter gradient (Fig. 4B, $P < 0.001$). Every micron increase in beam thickness gradient was associated with a 0.303 ± 0.024 µm (Fig. 4C, $P < 0.001$) increase in pore diameter gradient per 100-µm distance from the CRVT.

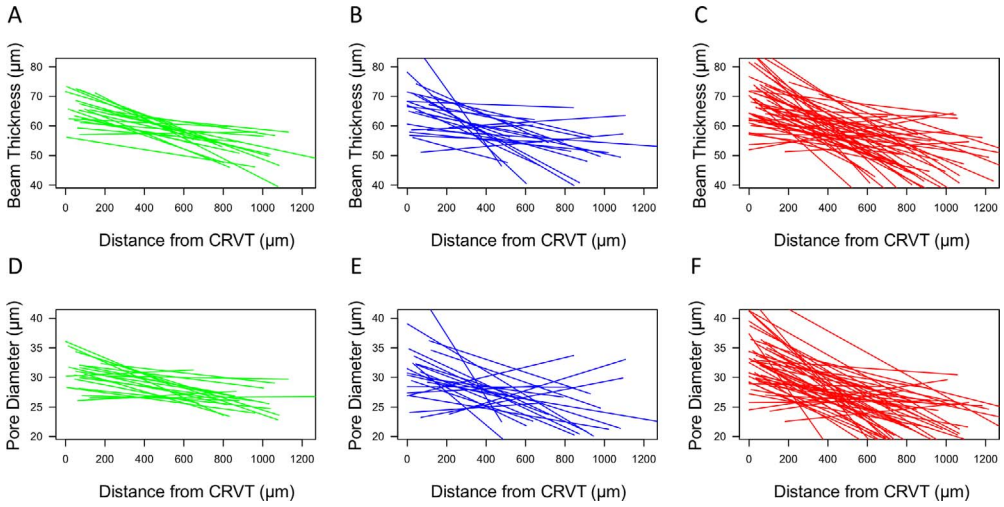

FIGURE 3. Best fit lines for beam thickness (**A–C**) and pore diameter (**D–F**) changes per distance from the CRVT for each eye. The start and end of the line segment signifies the distance over which LC microstructure was visible for that eye. *Green*, healthy; *Blue*, glaucoma suspect; *Red*, glaucomatous eyes.

Table. Comparison of the Gradients of LC Microstructure Changes (in Microns) With 100-μm Distance From CRVT Between Clinical Diagnostic Groups

	Beam Thickness, μm			Pore Diameter, μm		
	Estimate	**SE**	***P* Value**	**Estimate**	**SE**	***P* Value**
GS vs. H	−0.536	0.575	0.354	−0.392	0.295	0.189
GL vs. H	−1.132	0.503	**0.028**	−0.913	0.259	**0.001**
GL vs. GS	−0.596	0.492	0.229	−0.522	0.253	**0.043**

Bold font indicates $P < 0.05$. H, healthy; GS, glaucoma suspect; GL, glaucoma.

Discussion

In this study, we evaluate how 3D LC microstructural parameters, pore diameter, and beam thickness vary as a function of distance from CRVT. We demonstrate a decrease in beam thickness and pore diameter with distance from the CRVT. This decrease is more pronounced in glaucomatous eyes compared with healthy.

Our findings of decreased beam thickness and pore diameter with distance from the CRVT are in agreement with previous in vivo OCT characterization of LC microstructure, showing both pores and beams are smaller in the peripheral regions compared with central regions.[20] While it may appear counterintuitive that both beam thickness and pore diameter become smaller farther away from the CRVT, this is a result of increased pore density in the peripheral regions.[20] Ex vivo studies using scanning electron microscopy images of the LC also show a lower connective tissue fraction in the periphery, although beam thickness was not directly quantified.[21] However, the same ex vivo study show an increase in pore area in the periphery compared with the central regions. This difference in findings between ex vivo and in vivo studies of the LC may be explained by limitations of the techniques used in each study. Histology is prone to artifacts, especially with respect to the digestion of tissue prior to imaging of the LC. This can have the effect of digesting away thin beams between smaller pores in the periphery, giving the appearance of larger pores. Current OCT technology limits our ability to properly assess the peripheral LC, which is covered by thick prelaminar tissue and often goes beyond the BMO. Because it is impossible to assess the most peripheral regions of the LC using OCT, it is possible that pore diameter increases in the far periphery of the LC, as is suggested in a previous study through the analysis of a single eye.[22] This implies that there is an immediate drop in pore diameter in the area near the CRVT, but pores eventually get larger in the periphery.

As suggested above, the change in LC microstructure with distance from the CRVT may have a mechanical component.[23] The vessel wall within the CRVT contains collagen fibers mostly oriented in a perpendicular direction to the main axis of collagen fibers inside the LC. These perpendicular collagen fibers may play a role in resisting the deleterious effects of intraocular and intracranial pressures on the LC, and thus locations farther away from the CRVT are more prone to pressure insult and tissue remodeling. Therefore, a larger number of axons can pass through larger pores when they are adjacent to a supportive CRVT than when they are farther away. All these factors may contribute to the larger decrease in beam thickness and pore diameter, perhaps due to axonal loss and remodeling, with distance from the CRVT seen in the glaucoma subjects. Finally, areas closer to the CRVT are subject to repeated deformations through cardiac cycles, which might have a role in the general finding across all diagnostic groups that larger beams were observed at the CRVT margin.

Furthermore, it is important to assess whether the larger decrease in beam thickness and pore diameter versus distance from CRVT in glaucoma subjects are a result of glaucoma subjects having large beam thicknesses and pore diameters close to the CRVT, or loss occurring peripherally. We find that regions closest to the CRVT (represented by the intercept) had a strong influence on how the LC microstructure changes relative to the distance from the CRVT (Figs. 4A, 4B). For example, eyes with the greatest decrease in beam thickness with increased distance from the CRVT tend to have the thickest beams around the CRVT. These findings might be explained by the dynamic range of the measurements. Eyes with thicker beams near the CRVT also have more room to decrease in beam thickness with increased distance from the CRVT. Some of the differences between diagnostic categories, such as the larger variability in glaucomatous eyes, can be explained by the more variable intercept seen in these eyes (Fig. 3).

Interestingly, there is an association between beam thickness gradient and pore diameter gradient versus distance from CRVT (Fig. 4C). For example, eyes with large increases in beam thickness farther away from the CRVT also have large increases in pore diameter farther from the CRVT. This finding may be the result of an optimal ratio of beam thickness to pore diameter in response to remodeling.

As with any in vivo study of LC microstructure using OCT technology, we are limited to the region of visible LC, which is influenced by factors such as prelaminar tissue thickness and

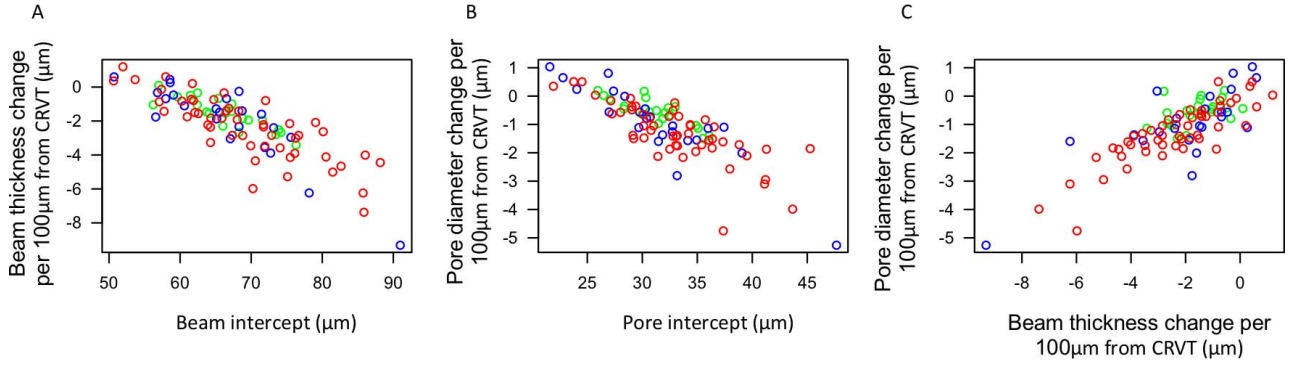

Figure 4. Scatterplot showing the relationship between (**A**) pore diameter and (**B**) beam thickness intercept with their respective gradients, as well as the (**C**) relationship between pore diameter gradient and beam thickness gradient versus distance from the CRVT. Gradient (unitless) denotes the micron change in lamina cribrosa microstructure per 100-μm distance from the CRVT. *Green*, healthy; *Blue*, glaucoma suspect; *Red*, glaucomatous eyes.

blood vessel shadowing. These factors are accounted for by including the percent of visible LC in the analysis. Additionally, as this is a cross sectional study, we cannot answer whether these changes reflect disease-related remodeling or are causative in the disease process.

In conclusion, we demonstrate in vivo that pore diameter and beam thickness in the LC are smaller with distance from the CRVT. The high variability observed in LC microstructural changes with distance from the CRVT in glaucomatous eyes points to the importance of considering the CRVT in mechanical modeling, as well as in vivo and ex vivo assessment of the LC.

Acknowledgments

Supported by grants from the National Institutes of Health (Bethesda, MD, USA): R01-EY013178, R01-EY025011, R01-EY011289, P30-EY008098, T32-EY017271; Eye and Ear Foundation (Pittsburgh, PA, USA); and Research to Prevent Blindness (New York, NY, USA).

Disclosure: **B. Wang**, None; **K.A. Lucy**, None; **J.S. Schuman**, Zeiss (R); **I.A. Sigal**, None; **R.A. Bilonick**, None; **L. Kagemann**, None; **T. Kostanyan**, None; **C. Lu**, None; **J. Liu**, None; **I. Grulkowski**, None; **J.G. Fujimoto**, Zeiss (R); **H. Ishikawa**, None; **G. Wollstein**, None

References

1. Burgoyne CF, Crawford Downs J, Bellezza AJ, Francis Suh J-K, Hart RT. The optic nerve head as a biomechanical structure: a new paradigm for understanding the role of IOP-related stress and strain in the pathophysiology of glaucomatous optic nerve head damage. *Prog Retin Eye Res*. 2005;24:39–73.
2. Miller KM, Quigley HA. The clinical appearance of the lamina cribrosa as a function of the extent of glaucomatous optic nerve damage. *Ophthalmology*. 1988;95:135–138.
3. Quigley HA, Broman AT. The number of people with glaucoma worldwide in 2010 and 2020. *Br J Ophthalmol*. 2006;90:262–267.
4. Wang B, Nevins JE, Nadler Z, et al. In vivo lamina cribrosa micro-architecture in healthy and glaucomatous eyes as assessed by optical coherence tomography. *Invest Ophthalmol Vis Sci*. 2013;54:8270–8274.
5. Inoue R, Hangai M, Kotera Y, et al. Three-dimensional high-speed optical coherence tomography imaging of lamina cribrosa in glaucoma. *Ophthalmology*. 2009;116:214–222.
6. Quigley HA, Addicks EM. Regional differences in the structure of the lamina cribrosa and their relation to glaucomatous optic nerve damage. *Arch Ophthalmol*. 1981;99:137–143.
7. Quigley HA, Addicks E, Green W, Maumenee A. Optic nerve damage in human glaucoma. II. The site of injury and susceptibility to damage. *Arch Ophthalmol*. 1981;99:635–649.
8. Kiumehr S, Park SC, Syril D, et al. In vivo evaluation of focal lamina cribrosa defects in glaucoma. *Arch Ophthalmol*. 2012;130:552–559.
9. Jonas JB, Fernández MC. Shape of the neuroretinal rim and position of the central retinal vessels in glaucoma. *Br J Ophthalmol*. 1994;78:99–102.
10. Jonas JB, Budde WM, Németh J, Gründler AE, Mistlberger A, Hayler JK. Central retinal vessel trunk exit and location of glaucomatous parapapillary atrophy in glaucoma. *Ophthalmology*. 2001;108:1059–1064.
11. Potsaid B, Baumann B, Huang D, et al. Ultrahigh speed 1050nm swept source/Fourier domain OCT retinal and anterior segment imaging at 100,000 to 400,000 axial scans per second. *Opt Express*. 2010;18:20029–20048.
12. Kraus MF, Potsaid B, Mayer MA, et al. Motion correction in optical coherence tomography volumes on a per A-scan basis using orthogonal scan patterns. *Biomed Opt Express*. 2012;3:1182.
13. Nadler Z, Wang B, Wollstein G, et al. Automated lamina cribrosa microstructural segmentation in optical coherence tomography scans of healthy and glaucomatous eyes. *Biomed Opt Express*. 2013;4:2596–2608.
14. Wang B, Nevins JE, Nadler Z, et al. Reproducibility of in-vivo OCT measured three-dimensional human lamina cribrosa microarchitecture. *PLoS One*. 2014;9:e95526.
15. Hildebrand T, Rüegsegger P. A new method for the model-independent assessment of thickness in three-dimensional images. *J Microsc*. 1997;185:67–75.
16. Doube M, Klosowski MM, Arganda-Carreras I, et al. BoneJ: free and extensible bone image analysis in ImageJ. *Bone*. 2010;47:1076–1079.
17. Abramoff MD, Magalhães PJ, Ram SJ. Image processing with ImageJ. *Biophotonics Int*. 2004;11:36–42.
18. Akaike H. A new look at the statistical model identification. *IEEE Trans Autom Control*. 1974;19:716–723.
19. R Development Core Team. *A Language and Environment for Statistical Computing*. Vienna: the R Foundation for Statistical Computing; 2008.
20. Nadler Z, Wang B, Schuman JS, et al. In vivo three-dimensional characterization of the healthy human lamina cribrosa with adaptive optics spectral-domain optical coherence tomography. *Invest Ophthalmol Vis Sci*. 2014;55:6459–6466.
21. Dandona L, Quigley HA, Brown AE, Enger C. Quantitative regional structure of the normal human lamina cribrosa: a racial comparison. *Arch Ophthalmol*. 1990;108:393–398.
22. Brown DJ, Morishige N, Neekhra A, Minckler DS, Jester JV. Application of second harmonic imaging microscopy to assess structural changes in optic nerve head structure ex vivo. *J Biomed Opt*. 2007;12:024029.
23. Flammer J, Orgül S, Costa VP, et al. The impact of ocular blood flow in glaucoma. *Prog Retin Eye Res*. 2002;21:359–393.

Investigative Ophthalmology & Visual Science